

A Large-scale Multimodal Study for Predicting Mortality Risk Using Minimal and Low Parameter Models and Separable Risk Assessment

Alvaro E. Ulloa Cerna, *Member, IEEE*, David P. vanMaanen, Linyuan Jing, Joshua V. Stough, Aalpen A. Patel, Christopher M. Haggerty, Brandon K. Fornwalt, and Marios S. Pattichis *Senior Member, IEEE*

Abstract—The majority of biomedical studies use limited datasets that may not generalize over large heterogeneous datasets that have been collected over several decades. The current paper develops and validates several multimodal models that can predict 1-year mortality based on a massive clinical dataset. Our focus on predicting 1-year mortality can provide a sense of urgency to the patients.

Using the largest dataset of its kind, the paper considers the development and validation of multimodal models based on 25,137,015 videos associated with 699,822 echocardiography studies from 316,125 patients, and 2,922,990 8-lead electrocardiogram (ECG) traces from 631,353 patients. Our models allow us to assess the contribution of individual factors and modalities to the overall risk. Our approach allows us to develop extremely low-parameter models that use optimized feature selection based on feature importance. Based on available clinical information, we construct a family of models that are made available in the DISIML package. Overall, performance ranges from an AUC of 0.72 with just ten parameters to an AUC of 0.89 with under 105k for the full multimodal model. The proposed approach represents a modular neural network framework that can provide insights into global risk trends and guide therapies for reducing mortality risk.

Index Terms—Large-scale Electronic Health Records Dataset, Low-parameter models, Separable models, Deep Learning, Machine Learning, Artificial Intelligence.

I. INTRODUCTION

The overwhelming majority of biomedical image and video analysis methods are evaluated on very limited datasets. With the evolution of Deep Learning systems with large parameters, the standard approach is to use transfer learning before retraining the models for application on biomedical datasets. Unfortunately, with the use of transfer learning, it is not clear what the derived models learn from unrelated datasets. The use of large biomedical datasets allows us to train relatively low-parameter models on unique biomedical tasks without the need for transfer learning.

The successful adoption of electronic health records (EHR) has made it possible to design studies with large multimodal

datasets. Furthermore, the use of large multimodal datasets can be used to develop generalizable models that can support clinical decision making through explanations supported by multiple modalities. Here, we want to consider laboratory measurements, ECG or other 1D signals, as well as imaging data.

Multimodal risk models based on large datasets can clearly benefit precision medicine (see [1], [2], [3]). On the other hand, there is a clear need for the models to support interpretability (see [4]) that includes all relevant predictors (or, conversely, clear explanations when relevant data input is excluded) [5]. Clinical decisions need to be explained in terms of the factors that influenced the decision as required by the European General Data Protection Regulation (<https://eugdpr.org/>). In the current paper, we develop a separable risk model that can be used to quantify how specific factors contribute to the overall risk.

We note that risk models are routinely used by physicians in clinical practice. These models do not predict time to death. Our risk models assess risk within a fixed period. Similarly, the Framingham risk score [6] provides a score for the risk of developing atherosclerotic cardiovascular disease or events within ten years. Other examples include the Pooled Cohort Equations [7] for atherosclerotic cardiovascular disease, and the Seattle Heart Failure score [8], for predicting mortality for 1, 2, and 3 years for patients who have suffered heart failure.

The current paper assesses mortality risk within a year. Thus, there is a natural urgency to the prediction since patients are much more likely to react to short-term rather than long-term risks. The current paper presents the first large-scale multimodal study focused on one-year mortality risk prediction based on EHR tabular data, echocardiography views, and ECG data. Our datasets are drawn from 25,137,015 videos in 699,822 echocardiography studies from 316,125 patients, and 2,922,990 8-lead ECG traces from 631,353 patients. Derived from this dataset, we consider a total of 28 combinations with three different methods for a total of $28 \times 3 = 84$ models for predicting one-year mortality. We are not aware of any published study that is comparable to this dataset. In general, previously published research uses a limited number of models on much smaller datasets.

Prior research on the use of large-scale video datasets has been primarily limited to echocardiography studies. In [9], the authors introduced the EchoNet-Dynamic, a video based system using 3D CNN and residual connections, for the as-

This project was funded, in part, under a grant with the Pennsylvania Department of Health (#SAP 4100070267).

Corresponding author: MP, Email: pattichi@unm.edu

AUC, LJ, CH and BF e-mails: [alvarouc, jinglinyan2008, chris.m.haggerty, brandon.fornwalt]@gmail.com, JV e-mail: joshua.stough@bucknell.edu, DV email: david@vanmaanen.us, AP email: aapatel@geisinger.edu

During the time of the study, AUC, DV, LJ, AP, JV, CH, and BF were with the Department of Translational Data Science and Informatics, Geisinger, PA 17822, USA. AUC and MP are with the Department of Electrical and Computer Engineering, University of New Mexico, NM 87131, USA.

assessment of cardiac function using a relatively large dataset of 10,030 annotated echocardiography videos. EchoNet-Dynamic performed very well at segmentating the left ventricle, estimating the ejection fraction, and then assessing heart failure due to a reduced ejection fraction. The authors verified that the system performance variance was comparable to what can be achieved with human observers. We note that EchoNet-Dynamic used the standard apical four-chamber view and also used weak supervision from expert human tracings (see Fig. 1 caption of [9]).

In [10], the authors used the EchoNet-Dynamic system to measure left ventricular wall thickness on 23,745 patients based on parasternal long-axis or apical 4-chamber view echocardiography videos. The authors reported that the system was able to detect subtle changes in left ventricular thickness that were then used to establish the causes of hypertrophy (e.g., cardiac amyloidosis or hypertrophic cardiomyopathy).

In [11], the authors fine-tuned the EchoNet-Dynamic system on a pediatric data set of 1,958 patients with 4,467 2-D apical 4-chamber and parasternal short axis echocardiography views to calculate the left ventricular ejection fraction based on select video frames. EchoNet-Peds was trained on 80% of the dataset and tested on the remaining 20% and found that the system could be used to identify pediatric patients with systolic dysfunction.

Compared to these earlier studies, we note that the current study is much larger, with data taken from 631,353 patients. Furthermore, instead of two views, video analysis is performed on 6 echocardiography views without any requirement for human supervision. Beyond the use of video models, our study developed 84 low-parameter multimodal models that are used to predict all-cause 1 year mortality as verified by electronic health records.

Our current paper builds on our prior research that developed a limited number of prediction models. In what follows, we provide a summary of our own related research. In terms of models, we developed one-year mortality risk models using only EHR tabular data in [12], electrocardiography (ECG) data with age and sex features in [13], and echocardiography with tabular data in [14]. In [12], we trained a Random Forest model with tabular information from patient demographics, blood test panels, and measurements from echocardiography studies. The random forest model yielded an area under the receiver operating characteristics curve (AUC) of 0.85, and was cross-validated within a 171,510 patient dataset. In [14], we considered the development of video models that were derived from 42,095 echocardiography studies, compared to the 699,822 echocardiography studies used in the current paper. In [14], our findings suggested that video data improved the performance of predicting 1-year mortality and that the model would benefit from more samples. Specifically, classification performance as a function of sample size did not reach a saturation point. In [13], we trained 1-D convolutional neural networks (CNN) with raw trace data from ECG that yielded an AUC of 0.88 in a held-out dataset of 168,914 patients. In [14], we trained 3-D CNNs with raw pixel data from echocardiography videos that yielded an AUC of 0.83 using video data only and 0.84 combining video and tabular EHR data. The video models

were cross-validated with a 34,362 patients dataset.

The current study aims to develop a family of separable risk models that can be used to predict one-year mortality based on clinical information that is available to us. Our focus on one-year mortality provides urgency for potential implementation of our work in clinical practice. We consider a large sample size of 631,353 patients to develop and validate our models. In terms of clinical information, we are using a multimodal dataset that includes echocardiography videos from multiple views, 8-lead ECG traces, and EHR tabular data. Our use of a multimodal dataset is significant because it represents a more complete picture of information that would be available for assessing mortality risk. Then, we develop a large number of prediction models that consider all possible combinations of the different modalities. For model assessment, we report AUC results from training on the individual modalities as well as their combinations. Given the size of our dataset, training required significant data storage and computational resources. It took approximately 45 days to train the models on an NVIDIA DGX-2 platform with 16 V100 32GB GPUs. Our development of separable risk assessment models allow us to quantify how different factors contribute to the overall risk. Specifically, our separable model allows us to assess the importance of each factor and provides an independent global assessment of the contribution of each factor. Overall, we develop low-parameter models that are trained on our large-scale datasets while avoiding biases associated with transfer learning methods. Among the many models considered here, we also build minimal models based on ranked factors. We then compare performance across models to demonstrate how the use of more complex models achieves more accuracy while simpler models achieve less accuracy while being easier to interpret.

The remainder of the paper is organized into four sections. In section II, we describe the dataset. In section III, we describe the proposed methodology. We then provide results and discussion in section IV and concluding remarks in section V.

II. LARGE-SCALE DATASETS

A. Electronic Health Records

Geisinger's EHR database contained demographics, vitals, labs, and measurements and findings from ECG and echocardiography studies from a total of 2,135,458 patients, of which 733,245 patients had at least an ECG or an echocardiography study. Geisinger's ECG database contained 2,922,990 ECGs from 631,353 patients acquired over 37 years (January 1984 to September 2021). Geisinger's echocardiography database contained 699,822 studies (25,137,015 videos) from 316,125 patients performed over 23 years (February 1998 to September 2021). Each study included the date, a findings report, and patient identifier information. Geisinger's Phenomics Initiative database has modeled these data along with multiple clinical features into a tabular format that included human-derived echocardiography and ECG measurements. We then combined all datasets and merged them based on echocardiography encounters. We assigned the latest measurements up to a year prior to the echocardiography encounter. If the measurement

TABLE I

LIST OF VARIABLES FOR EACH DATA MODALITY. UNITS ARE GIVEN IN BETWEEN PARENTHESES. BINARY VARIABLES DO NOT HAVE UNITS.

Clinical EHR
Demographics: White, Male, Ever smoked, Age (years) Vitals: Body mass index (kg/m ²), Diastolic Pressure (mmHg), Systolic Pressure (mmHg), Heart Rate (beats/min), Height (cm), Weight (kg) Lab: HbA1C (%), Bilirubin (mg/dL), BUN (mg/dL), Cholesterol (mg/dL), Creatine kinase-MB (ng/mL), Creatinine (mg/dL), C-reactive protein (mg/L), D-dimer (μg/mL), Glucose (mg/dL), High-density lipoprotein (mg/dL), Hemoglobin (g/dL), Lactate dehydrogenase (U/L), Low-density lipoprotein (mg/dL), Lymphocytes (%), Potassium (mmol/L), Pro-BNP (pg/mL), Sodium (mmol/L), Troponin I (ng/mL), Troponin T (ng/mL), Triglyceride (mg/dL), Uric acid (mg/dL), Very-low-density lipoprotein (mg/dL), eGFR (mL/(min 1.73 m ²)),
Echocardiography
Aortic valve: No regurgitation, Mild regurgitation, Moderate regurgitation, Severe regurgitation, Regurgitation not assessed, No stenosis, Mild stenosis, Moderate stenosis, Severe stenosis, Stenosis not assessed, Insufficiency deceleration slope (cm/sec ²), Insufficiency max velocity (cm/sec), Area (cm ² (I,A)), Flow vel-time integral (cm), Flow distal max vel (cm/sec), Flow distal mean vel (cm/sec), Mean pressure gradient (mmHg) Mitral valve: No regurgitation, Mild regurgitation, Moderate regurgitation, Severe regurgitation, Regurgitation not assessed, No stenosis, Mild stenosis, Moderate stenosis, Severe stenosis, Stenosis not assessed, Regurgitation max vel (cm/sec), A-point flow max vel (cm/sec), E-point flow max vel (cm/sec), P1/2t max vel (cm/sec), Deceleration slope (cm/sec ²), Deceleration time (sec) Pulmonary valve: No regurgitation, Mild regurgitation, Moderate regurgitation, Severe regurgitation, Regurgitation not assessed, No stenosis, Mild stenosis, Moderate stenosis, Severe stenosis, Stenosis not assessed, Tricuspid valve: No regurgitation, Mild regurgitation, Moderate regurgitation, Severe regurgitation, Regurgitation not assessed, No stenosis, Mild stenosis, Moderate stenosis, Severe stenosis, Stenosis not assessed, Regurgitation max vel (cm/sec), Left ventricle: End-diastolic vol (AP2)* (ml), End-diastolic vol (AP4)* (ml), End-diastolic vol (AP2)** (ml), End-diastolic vol (AP4)** (ml), End-systolic vol (AP2)* (ml), End-systolic vol (AP4)* (ml), End-systolic vol (AP2)** (ml), End-systolic vol (AP4)** (ml), V1 vel-time integral, V1 max vel (cm/sec), V1 mean vel (cm/sec), Diastole area (AP2) (cm ²), Diastole area (AP4) (cm ²), Systole area (AP2) (cm ²), Systole area (AP4) (cm ²), Internal diastole dimension (cm), Internal systole dimension (cm), Diastole length (AP2) (cm), Diastole length (AP4) (cm), Systole length (AP2) (cm), Systole length (AP4) (cm), Outflow tract area (cm ²), Outflow tract diameter (cm), Diastole posterior wall thickness (mm), Ejection fraction (%) Left atrium: Left atrium dimension (cm), Left atrium vol (AP2)* (ml), Left atrium vol (AP4)* (ml) Pulmonary artery: V2 max vel (cm/sec), Acceleration slope (cm/sec ²), Acceleration time (sec), Other: Aortic root diameter (cm), Interventricular septum thickness (cm), Pulmonary R-R interval (sec), Right atrial end-systolic mean pressure (mmHg), Right ventricle dimension at end-diastole, Ascending aorta diameter (cm), Normal diastolic function,
Electrocardiography (ECG)
Findings: Acute myocardial infarction, Atrial fibrillation, Atrial flutter, Complete heart block, Early repolarization, Fascicular block, First-degree block, Intraventricular block, Incomplete left bundle-branch block, Incomplete right bundle-branch block, Ischemia, Left axis deviation, Left bundle-branch block, Low QRS voltage, Left ventricular hypertrophy, Nonspecific ST changes, Nonspecific T-wave changes, Normal, Other bradycardia, Premature atrial contractions, Pacemaker, Poor tracing, Previous infarct, Previous anterior myocardial infarction, Prolonged QT, Premature ventricular contractions, Right axis deviation, Right bundle-branch block, Second-degree atrioventricular block, Sinus bradycardia, Supraventricular tachycardia, Tachycardia, T-wave inversion, Ventricular tachycardia, Measurements: R axis (degrees), PR interval (sec), P axis (degrees), QRS duration (sec), QT (msec), QTC (msec), T axis (degrees), Ventricular rate (beats/min), Average RR interval (msec)

* Obtained by modified ellipsoid technique

** Obtained using a single plane ellipsoid technique

was older than 1 year, it was considered missing. This approach was also applied to the ECG dataset, where for every echocardiography encounter we linked a past ECG no older than a year.

The measurements were cleaned from input errors that had resulted in entries that were not physiologically possible. In cases where we could not establish limits, we removed extreme outliers. Here, we defined extreme outliers as values that were more than three standard deviations from the mean, or below the 25th percentile minus 3 interquartile ranges, and similarly for the 75th percentile. After removing the outlier values, we set the values as missing.

We applied a Multiple Imputation by Chained Equations (MICE) [15] for handling missing values. We note that the effect of replacing the missing values has a minimal effect on the model AUC [16], [12].

The diastolic function was classified as normal or dysfunction (I, II, III or unspecified). We define our one year mortality risk based on the date of the echocardiography study. To establish the patient status (dead/alive), we used last exam, or a confirmed death date within our national death databases.

By definition, patients in the “Alive” (negative) class were followed for over a year (i.e., had a last-known living encounter more than one year after the echocardiography study), while patients in the “Deceased” (positive) class were followed for less than a year (until death). Thus, patients in the negative class have longer follow-up time compared to patients in the positive class and contributed to more available echocardiography studies. The 539,689 studies that fell in the alive class belonged to 248,250 unique patients (2.2 studies per patient), and the 68,049 studies from the deceased class belonged to 46,031 patients (1.5 studies per patient). To avoid biasing the results to patients in the “Alive” class, we report performance metrics after selecting a random study per patient.

B. Echocardiography video data

An echocardiography study typically consists of 20–30 ultrasound videos containing multiple views of the heart and vessels with different orientations. In our previous study [14], we extracted videos with known views. In the current study, only 28% of all extracted videos included a description of the source view (e.g. “AP4” indicating a four chamber view). To overcome this and maximize the number of videos used to train mortality models, we trained view classifier models with the view-labeled data available in the training set.

From an echocardiography study, we kept only the videos from the parasternal long axis view, the apical two-, four- and five-chamber views, and the basal and mid-ventricular short-axis views. These views are regarded as the most useful by cardiologists because they capture a large part of the heart’s anatomy. Furthermore, as documented in [14], these views gave the best performance for predicting the risk of one-year mortality, and including several millions of videos from additional views was deemed infeasible with minimal anticipated benefit. To reduce storage requirements, the videos were compressed using the default Motion-JPEG settings available in OpenCV.

C. Electrocardiography trace data

An ECG test consists of a 10-second recording of electrical potential in the heart for 12 leads at a sampling rate of either 250Hz or 500Hz. For this study, we retained the digital voltage data from the 8 non-derived leads (I, II, V1-V6). For ECG data sampled at 250Hz, we used interpolation to extend the dataset to 500Hz. We extracted the trace data from Geisinger's MUSE (GE Healthcare) and stored it in the lightning memory-mapped database format (<https://dbdb.io/db/lmdb>).

D. Training, Validation, and Testing of the Multimodal Model

Starting from all patients with at least an ECG or an echocardiography study (733,245 patients), we randomly assigned 80% of the patients to the training set, and the rest to the test set. All of our results are reported on the test set.

We train the whole multimodal model in three stages. First, we train six view classifier models (one for each view) in a one-vs-all procedure and collect videos from the desired view to feed the next stage. Second, we train the mortality models with convolutional neural network (CNN) architectures (echocardiography videos and ECG traces) independently. The echocardiography video models are trained with 517,348 echocardiography studies found within the training patient list. We train one video model per view with known-view videos and use the model to predict the view of unlabeled-view videos by requiring at least 90% positive predicted values in the training set. The ECG models are trained with 2,339,622 resting 8-lead ECGs within the training patient list. Lastly, we transfer the individually trained CNN models to the proposed multimodal model, where we train again the full model with the 517,348 echocardiography encounters to obtain the feature importance coefficients and the polynomial transformations.

For training, we use the Adam optimization method [17] to minimize the binary cross-entropy loss. In all training stages, we monitor the training progress with a subset of the training set, i.e the internal validation set. The validation set is composed of 5% of the positive cases and an equal number of negative cases, both of which were randomly selected. If the internal validation loss does not decrease for more than 10 epochs, we stop the training and recover the model weights at the minimum validation loss [18].

Here we note that to train the logistic regression and XGB multimodal models, we use the predicted risk scores from each echocardiography video and the ECG traces as input features. However, the proposed model allows us to train using the scalar features along with the echocardiography videos and ECG trace data.

We standardize each scalar factor in the range of $[-1, +1]$. This is done using:

$$x_{\text{normalized}} = 2 \cdot \frac{x - x_{i,\min}}{x_{i,\max} - x_{i,\min}} - 1, \quad (1)$$

where $x_{i,\min}$ denotes the minimum value for x , and $x_{i,\max}$ denotes the maximum value for x . We also weigh the error contributions from each class based on the number of samples in each class to account for sample imbalance. This is given by

$$\text{Error weight for } i\text{-th class} = \frac{N}{NOC * N_i},$$

where N denotes the total number of samples in all classes, N_i denotes the number of samples in class i , and $NOC = 2$ denotes the number of classes. Here, we use a weight of 4.4 for the positive cases and 0.6 for the negative cases.

To train, we gather all encounters from patients in the training set. For testing, we select a random echocardiography encounter per patient to avoid biasing the test results toward patients with more encounters.

We implemented all the experiments with the Tensorflow Docker image *tensorflow/tensorflow:2.8.0-gpu-jupyter* on an NVIDIA DGX-2 platform with 16 V100 32GB GPUs.

III. METHODS

We present the multimodal processing system in Fig. 1. Our system is used to process routine clinical, echocardiography, and ECG data (including multiple videos, traces, measurements, and findings). We use CNN models to process the videos and the ECG traces as described below. We use a separable risk model (SRM) system to combine the results from the different modalities to predict one-year mortality. The SRM produces a risk score that represents the likelihood of mortality within a year. We note that this retrospective study was approved by the Geisinger Institutional Review Board and performed with a waiver of consent. The work falls under the AI in cardiology study (Machine Learning for Data-Driven Precision Medicine) with GIRB# 2019-0610.

We provide a brief summary of the different modality inputs to the SRM. We have 33 variables from routine clinical data stored in the EHR. They include demographics (age, sex, race, smoking status), vitals (body mass index (BMI), blood pressures, etc.), and labs (cholesterol, hemoglobin, etc.). A list of the 33 variables is given in Table I. We have 92 inputs associated with the measurements and findings from echocardiography as given in Table I. The measurements and findings are derived from up to 30 different echocardiography views, but in this study we select six views that include elements of the left ventricle, left atrium, right ventricle, and aortic and mitral valves: the parasternal long axis view, the apical two, four and five chamber views, and the basal and mid-ventricular short-axis views. The videos were aligned to start at the peak of the R-wave of the QRS complex, zero-padded or cropped to 2 seconds, sampled at 30 frames per second using linear interpolation, and downsampled to 109×150 pixels. In [14], these six echocardiography views were among the best performing for one-year mortality prediction and used a 3D CNN architecture, and we adopt that architecture here. The ECG traces were derived from standard clinical 12-lead ECG acquisitions. Specifically, we retained 10-second recordings for each of the 8 non-derived leads, resampled at 500Hz to ensure consistency. We use a multichannel 1D CNN architecture to process the ECG signal as described in [19]. We use 43 ECG-derived measurements and findings, confirmed by cardiologists, as described in Table I.

The SNN uses a linear combination of the results from the different modalities to produce a single score. For each one of the continuous variables, we use separable polynomial transformations as we will describe below. For binary variables, the

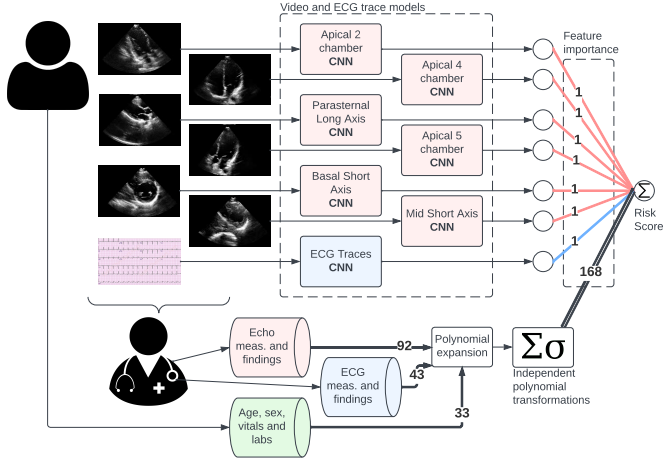


Fig. 1. Multimodal system diagram. The system uses echocardiography ('Echo') videos from 6 views (top-left), ECG traces from multiple channels, Echo and ECG measurements and findings, and basic clinical data (age, sex, vitals, and labs). The Echo and ECG measurements and findings are supplied by the physician. 3D CNN models are used for processing the videos. A multichannel 1D CNN model is used for training on the ECG traces. The Separable Neural Network system (SNN) is used to process the contributions from the different inputs. The echocardiography videos yield a total of six features (red lines), the ECG traces yield one feature (blue line), and the structured data contribute 168 features (black line).

video scores derived from the 3D CNNs, and the ECG scores derived from the multichannel 1D CNN, we assign a single weight for each one. Thus, the SNN can be used to directly assess the importance of the processed video and ECG data as well as study-derived measurements and findings.

We provide a detailed description of the transformations and the multimodal model in section III-A. In section III-B, we describe how the proposed method supports interpretability by ranking features based on their corresponding risks. Here, we note that the interpretability of the most significant features will be further expanded in the results of section IV.

A. Multimodal Models for Mortality Risk Prediction

We begin by differentiating categorical factors (e.g., sex), continuous clinical factors (e.g., heart-rate), and risk factors associated with specific modalities (e.g., ECG). We will construct different models based on the labs, the imaging data, and the ECG. We will then consider all possible combinations of the different modalities.

We first define all the variables. We write $X = [x_1, x_2, \dots, x_r]^T$ for r scalar factors. For the 6 views associated with video analysis, we have $V = [v_1, v_2, \dots, v_6]^T$. Then, for the combined outputs for all views, we write $M_V = [m_{v1}(v_1), m_{v2}(v_2), \dots, m_{v6}(v_6)]^T$. We let m_t denote the output associated with the ECG.

We consider a separable model where a polynomial transformation is applied to each factor separately. Thus, the list of all polynomial transformations is given by:

$$P(X) = [p_1(x_1), p_2(x_2), \dots, p_r(x_r)]^T,$$

where

$$p(x_i) = \begin{cases} \sigma(a_0 + a_1x_i + a_2x_i^2 + a_3x_i^3 + \dots) & \text{if } x_i \in \mathbb{R} \\ x_i & \text{if } x_i \in \{0, 1\} \end{cases}$$

and $\sigma(x) = 1/(1 + \exp(-x))$. Here, we are inspired by the use of polynomial regression for linear models to use polynomial transformations to describe the non-linear relationship between risk and each input feature. We note that polynomial transformations require relatively few parameters for describing non-linear relationships. For third-degree polynomials, we need just 4 parameters to fit most non-linearities. As we shall describe in the results, there is some evidence that we may not need a higher-order polynomial for modeling risk from single features. In our DISIML package, we allow for a higher degree selection, which can be optimized via hyper-parameter search.

We use a weighted sum of the contributions from each polynomial based on:

$$W_p P(X) = w_1 p_1(x_1) + w_2 p_2(x_2) + \dots + w_r p_r(x_r), \quad (2)$$

where $W_p = [w_1, w_2, \dots, w_r]$. Here, we note that the direction of effect in $p_i(x_i)$ could cause the sign of w to flip and provide two solutions, since $\sigma(-x) = 1 - \sigma(x)$.

We thus have that the multimodal risk models are given by:

$$\begin{aligned} m(X, M_V, m_t) &= \sigma(W P_{\text{all}}(X, M_V, m_t) + b) \\ &= \sigma(W_p P(X) + W_v M_V + w_t m_t + b) \end{aligned} \quad (3)$$

where $P_{\text{all}}(X, M_V, m_t) = [P(X), M_V, m_t]^T$, $W_v = [w_{v1}, w_{v2}, \dots, w_{v6}]$ represents the weights associated with echocardiography views, w_t represents the weight associated with the ECG, $W = [W_p, W_v, w_t]$, and b represents the bias term.

B. Separable Models

Using (3), we compute the final score using:

$$\begin{aligned} m(X, M_V, m_t) &= \sigma(W P_{\text{all}}(X, M_V, m_t) + b) \\ &= \frac{1}{1 + \exp(-W P_{\text{all}}(X, M_V, m_t) - b)}. \end{aligned} \quad (4)$$

To simplify the notation, let $p_{\text{mort}} = m(X, M_V, m_t)$ denote the mortality probability. We note that $p_{\text{mort}} = \sigma(\text{logit}(p_{\text{mort}}))$ where $\text{logit}(\cdot) = \sigma^{-1}(\cdot)$ represents the inverse of $\sigma(\cdot)$. We thus have:

$$\begin{aligned} W P_{\text{all}}(X, M_V, m_t) + b &= \text{logit}(p_{\text{mort}}) \\ &= \log \left(\frac{p_{\text{mort}}}{1 - p_{\text{mort}}} \right) \end{aligned} \quad (5)$$

where $p_{\text{mort}}/(1 - p_{\text{mort}})$ represents the odds ratio. Specifically, the product $W P_{\text{all}}(X, M_V, m_t) + b$ provides the log-odds of a mortality event [20]. Next, to separate out the risk contribution for the i -th factor, exponentiate both sides of eq. (5) to get:

$$\text{Odds-ratio} = C \cdot \exp(w_i p_i(s)), \quad (6)$$

where C represents the combined contribution from the rest of the features, w_i represents the weight from any one of the features, p_i represents any one of the variables, and s denotes

any one of the contributing variables or modalities. From eq. (6), it is clear that w_i can be used to understand the contribution of the i -th feature to the odds ratio of the entire model. In order to quantify the contribution of each feature, we rank their corresponding weights as given by: $|w|_{(1)} \geq |w|_{(2)} \geq \dots \geq 0$. To quantify the sensitivity of the risk model for a specific feature, we look at the change from $\exp(w_s p_s(s))$ to $\exp(w_s p_s(s + \Delta s))$ where Δs is used to describe a large change in s .

IV. RESULTS AND DISCUSSION

We begin with a discussion of the most significant features in section IV-A. We then proceed with interpretability results for the most significant features in section IV-B. We provide two minimal model examples of our proposed separable neural network in section IV-C. We provide comprehensive results for different modalities and our multimodality system in section IV-D.

A. Significant features

We summarize the results for the most significant features for the different models in Table II. We begin our discussion with the most significant features across modalities. We then discuss the most significant features for each modality in more detail.

As expected for a survival model, age dominates all other features in the basic EHR model. For the multimodal model, age remains the second most important feature.

The outputs of the CNNs dominate in the echocardiography, ECG, and multimodal model, as opposed to the measurements and findings in both modalities. For the echocardiography model, the outputs of the 3D CNN models associated with the two apical views dominate all others. For the ECG and multimodal models, the output of the multichannel 1D CNN associated with the ECG traces is the most significant feature.

Overall, for the echocardiography modality, the 3D CNN outputs associated with three views (apical 4 and 2 chambers, and parasternal long-axis) are among the top 5 most important features. The remaining two most significant features include the presence of severe tricuspid stenosis (a finding), and tricuspid regurgitation maximum velocity (TRMV, a measurement). We recall TRMV measures the maximum velocity of blood flowing backwards from the right ventricle into the right atrium. The TRMV is an indirect measure of pulmonary artery systolic pressure which makes it a marker of pulmonary hypertension. The increased mortality risk may be due to pulmonary hypertension as discussed in [12], which supports clinical interpretability of the model.

For the ECG modality model, the output of the multichannel 1D CNN applied to the ECG trace data is the most important feature with a coefficient that is 5 times higher than the second most important. The remaining top 5 features comprise standard ECG measurements of features or intervals. We also note that in [13], ECG measurements and findings did not contribute to the model performance as much as the trace data alone.

For the multimodal model, as mentioned earlier, the output of the ECG trace data was the most significant feature.

Unfortunately, it is difficult to provide a clinical interpretation of exactly what is being measured by the ECG analysis system. A previous attempt at interpreting saliency maps in [13] for ECG traces was inconclusive. Similarly, for video data, in our previous study [14], we found that cardiologists could not use the occlusion maps to improve their predictive ability using video data, relying on the risk scores instead. Overall, for mortality risk prediction, the dominance of the ECG and video signal processing system in both performance and feature ranks suggests that one-year mortality models benefit from incorporating raw data signals. Lastly, the polynomial model based on lymphocytes (a lab measurement) was found to be as important as the video models associated with the apical 4 and 2 chambers views. Lymphocytes are part of the immune system and deviations may indicate the presence of a wide range of diseases such as infection, or the presence of pathology within the immune system.

B. Risk model assessment for individual features

In Fig. 2, we show the risk functions associated with the 10 most significant non-binary clinical features associated with the multimodal model. Each risk function represents the contribution of $\sigma_s(s)$ in the multimodal model of eq. (6). Here, we do not show risk functions for the CNNs. In what follows, we interpret the most significant features.

Based on the risk function diagrams of Fig. 2, we note that our third-order polynomial model captures some significant non-linearities. It is clear from the risk trends that a linear model would be inadequate for many features. At the same time, for any given risk level, we never have more than two feature values that map to that risk value. Here, we note that our cubic model would have allowed up to three feature values that map to the same risk value. Hence, the fact that this never happens provides some evidence that we may not need higher order polynomials to capture the trends.

We begin our analysis with the age factor (see Fig. 2(a)). We can clearly see mortality increases with age. Age has a weight coefficient of 2.1 (see Table II). This implies an 8-fold ($8 \approx e^{2.1}$) increase in the odds ratio between the minimum age of 18 and the maximum age of 98 years old.

The normal range for lymphocytes is between 20% and 40%, which is the range where our analysis shows the risk is the lowest (see Fig. 2(b)). Known as lymphocytopenia, decreased lymphocyte levels may indicate a severe infection, such as sepsis, which is the most common cause of death in hospitals in the US [21].

Following a U-shaped risk trend, lactate dehydrogenase (Fig. 2(c)) shows the lowest risk at normal range values, between 105 to 333. Similarly, the normal range for bilirubin (Fig. 2(d)) is 0.1 to 1.2.

For hemoglobin, we observed a rapid decline in risk for higher values (Fig. 2(e)). This could indicate the higher mortality rate of end-stage anemic patients. We also note that slightly different normal ranges are expected for males and females. For future iterations of this model we could add a hemoglobin and sex interaction term to assess whether the interaction coefficient is of significant importance.

TABLE II

TOP FIVE FEATURES WITH THEIR CORRESPONDING COEFFICIENTS FOR DIFFERENT MODALITIES. THE MODELS WERE TRAINED BASED ON DATA ALIGNED WITH ECHOCARDIOGRAPHY ENCOUNTERS.

Rank	Single Modality						Multimodal	
	EHR		Echocardiography		ECG		EHR+Echocardiography+ECG	
	Variable	Coef.	Variable	Coef.	Variable	Coef.	Variable	Coef.
1	Age	3.8	Apical 4 chamber*	2.4	ECG traces	4.8	ECG traces	2.3
2	Heart rate	2.1	Apical 2 chamber*	1.9	R axis	-0.9	Age	2.1
3	Hemoglobin	1.8	Severe Tricuspid stenosis	1.4	QRS duration	-0.8	Apical 4 chamber*	1.5
4	eGFR	1.5	Parasternal long axis*	1.3	T Axis	-0.8	Apical 2 chamber*	1.4
5	Lymphocytes	-1.4	Tricuspid regurgitation max velocity	1.2	QTC	-0.8	Lymphocytes	1.4

*Video data

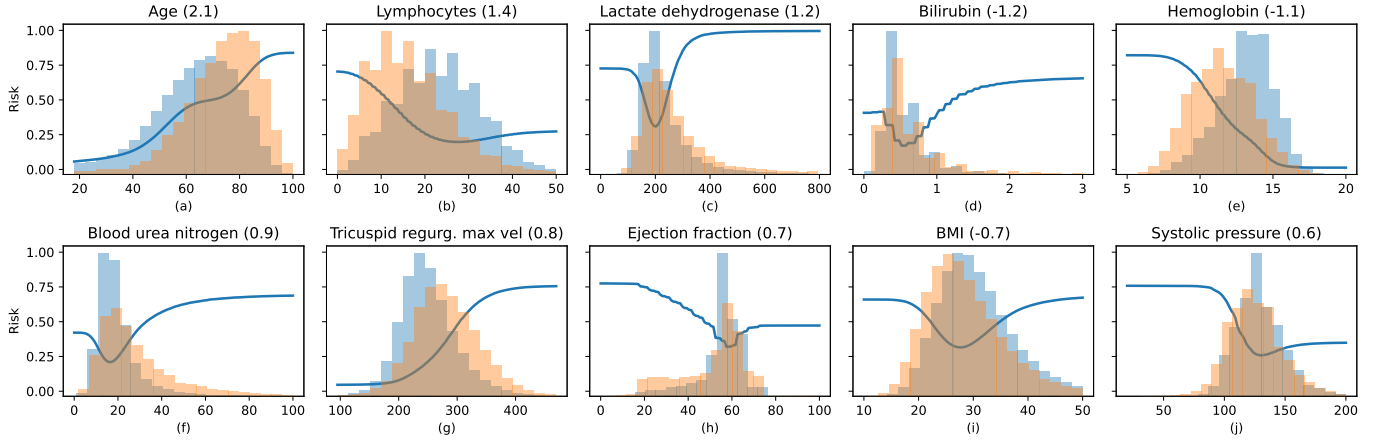


Fig. 2. Separable risk functions for the 10 most significant clinical, non-binary features. The risk functions are shown in blue. The normalized histograms of the survivors are shown in light blue. The normalized histograms of the non-survivors appear in orange. When the two histograms overlap, the histograms appear light brown. Risk functions for: (a) age in years, (b) lymphocytes in percent, (c) lactate dehydrogenase in units per liter, (d) bilirubin in milligrams per deciliter, (e) hemoglobin in grams per deciliter, (f) blood urea nitrogen in milligrams per deciliter, (g) tricuspid regurgitation maximum velocity in centimeters per second, (h) left ventricular ejection fraction in percent, (i) BMI in kilograms per meter squared, and (j) systolic blood pressure in millimeters of mercury. For each risk function, the weight for each feature is given in the title of the graph. If the coefficient is negative, the risk function is corrected to normalize the graph to higher values for higher risk.

The risk trend for blood urea nitrogen (Fig. 2(f)) was also U-shaped with the lowest risk at normal range values, 6 to 24.

We have a strong, positive trend for increases in the TRMV (see Fig. 2(g)). Based on our prior discussion on the TRMV, this trend is to be expected and compatible with pulmonary hypertension being strongly linked to mortality.

The model yielded a U-shaped trend for the left ventricular EF (see Fig. 2(h)). This trend agrees with the findings described in [22]. It is important to recognize that the majority of the patients fall within the non-linear trend region and thus it would be a false assumption to suggest a linear trend for the entire EF region. Moreover, the performance drop from 0.76 (using the proposed model) to 0.73 (using logistic regression), shown in the first row of Table V, also suggests that non-linearity improves performance. We recall that EF denotes the percentage of blood that leaves the left ventricle chamber during contraction. Based on the current American Heart Association guidelines (reviewed as of May 31, 2017), normal EF values are between 50% and 70%. We can clearly see that our model correctly modeled this range as low-risk (see Fig. 2(h)). On the other hand, high EF may be a

marker of a hyperdynamic heart failure with preserved ejection fraction [22]. Yet, for heart failure, low EF is well recognized as a poor prognosticator.

The model also yielded a U-shaped trend for BMI with an optimal value between 25 and 30 (see Fig. 2(i)). While current guidelines from the World Health Organization, define a normal BMI range as 18.5 to 24.9, a recent study [23] suggests that for adults older than 65 BMIs lower than 23 or higher than 33 were the most harmful. Geisinger's clinical population has a median age of 66, which aligns better with [23].

We note that there is a notable increase in risk for low values of the systolic pressure (see Fig. 2(j)). There are two possible interpretations for this trend. First, we note that high blood pressure may not lead to 1-year mortality. Instead, high blood pressure results in long-term cumulative effects such as renal and heart failure which results in an increased risk for longer-term mortality. Second, we note that low blood pressure may be a marker of cardiac decompensation. Here, we note that cardiac decompensation is more acutely associated with hospitalization and death. Clearly, in order to fully understand

the trend, further study will be needed, taking into account how patient medications affect blood pressure.

C. Minimal Models

We also consider two minimal models that avoid any features that are based on ECG or echocardiography exams. For the first minimal model, we consider common variables that can be monitored at home with a weight scale and a blood pressure monitor: age, heart rate (HR), BMI, systolic (SP) and diastolic (DP) blood pressures. For the second minimal model, we selected the top 5 scalar features from the multimodal model that were not ECG or echocardiography based features: age, lactate dehydrogenase (LDH), bilirubin (Bil), lymphocytes (Lym), and hemoglobin (Hgb). As we did for all other models, we standardize each factor in the range of -1 to +1. For completeness, we provide the min and max values in Table III.

The mortality risk based on the first minimal model gave:

$$\begin{aligned} \text{Risk} = \sigma (& \\ & 3.62 \sigma (1.82 \cdot \text{Age}^3 - 0.53 \cdot \text{Age}^2 + 0.66 \cdot \text{Age} - 0.09) \\ & + 2.81 \sigma (1.53 \cdot \text{HR}^3 + 0.17 \cdot \text{HR}^2 + 0.52 \cdot \text{HR} - 1.35) \\ & + 1.60 \sigma (-0.42 \cdot \text{BMI}^3 + 1.96 \cdot \text{BMI}^2 - 0.30 \cdot \text{BMI} - 1.48) \\ & + 1.37 \sigma (-2.98 \cdot \text{DP}^3 - 1.26 \cdot \text{DP}^2 - 1.42 \cdot \text{DP} - 1.68) \\ & + 2.75 \sigma (-0.34 \cdot \text{SP}^3 + 0.86 \cdot \text{SP}^2 - 0.09 \cdot \text{SP} + 0.21) \\ & - 5.09). \end{aligned} \quad (7)$$

In eq. (7), we have normalized the expression to give positive weights for the final layer using $\sigma(-x) = 1 - \sigma(x)$. Based on the last layer coefficients, we have the features ranked in the order of: age, heart rate, systolic pressure, BMI, and diastolic pressure. However, the most exciting result is that this simple model gave an AUC of 0.78, which approximates the performance of far more sophisticated models discussed in section IV-D.

TABLE III
SUMMARY OF MINIMUM AND MAXIMUM VALUES USED FOR
NORMALIZING FEATURES FOR THE MINIMAL MODELS (SEE EQ. (1)).

	Units	Min	Max
Age	years	18	98
Heart Rate (HR)	beats per minute	40	150
BMI	kg/m ²	14.4	76.3
Diastolic Pressure (DP)	mmHg	32	120
Systolic Pressure (SP)	mmHg	72	213
Lymphocytes (Lym)	percent	1	91
Lactate Dehydrogenase (LDH)	units/L	74	2513
Bilirubin (Bil)	mg/dL	0.1	10.4
Hemoglobin (Hgb)	g/dL	6.3	19

TABLE IV
SUMMARY STATISTICS ON ALL ECHOCARDIOGRAPHY STUDIES, WHERE
THE PATIENT SURVIVED OR DIED WITHIN A YEAR OF THE STUDY. WE
SHOW THE STUDY AND PATIENT COUNTS; FEATURES AVERAGES,
STANDARD DEVIATIONS (IN PARENTHESIS) AND INTERQUARTILE RANGES
(IN BRACKETS).

	Alive		Deceased	
# Echo studies	539,689		68,049	
# Patients	248,250		46,031	
	Mean (SD)	IQR	Mean (SD)	IQR
Age	64 (16)	[54, 75]	73 (14)	[65, 84]
Heart Rate	75 (15)	[64, 83]	80 (17)	[68, 89]
BMI	31 (8)	[26, 35]	29 (9)	[24, 33]
Diastolic Press.	73 (12)	[64, 80]	68 (13)	[60, 76]
Systolic Press.	129 (19)	[117, 140]	125 (22)	[110, 139]
LDH	251 (266)	[173, 263]	320 (387)	[189, 325]
Hemoglobin	15 (45)	[12, 14]	12 (33)	[10, 13]
Bilirubin	0.56 (0.58)	[0.30, 0.70]	0.81 (1.64)	[0.30, 0.80]
Lymphocytes	23 (10)	[16, 30]	17 (12)	[9, 22]

The mortality risk for the second model gave:

$$\begin{aligned} \text{Risk} = \sigma (& \\ & 3.76 \sigma (1.95 \cdot \text{Age}^3 - 0.80 \cdot \text{Age}^2 + 0.59 \cdot \text{Age} - 0.71) \\ & + 2.40 \sigma (-1.38 \cdot \text{Lym}^3 - 0.75 \cdot \text{Lym}^2 - 2.03 \cdot \text{Lym} - 1.58) \\ & + 1.33 \sigma (-2.33 \cdot \text{LDH}^3 - 6.18 \cdot \text{LDH}^2 - 2.18 \cdot \text{LDH} + 0.93) \\ & + 2.38 \sigma (1.47 \cdot \text{Bil}^3 + 1.22 \cdot \text{Bil}^2 - 0.52 \cdot \text{Bil} - 1.96) \\ & + 2.27 \sigma (3.13 \cdot \text{Hgb}^3 + 1.56 \cdot \text{Hgb}^2 + 1.84 \cdot \text{Hgb} + 1.33) \\ & - 3.40). \end{aligned} \quad (8)$$

In eq. (8), we have the features ranked in the order of: age, lymphocytes (Lym), bilirubin (Bil), hemoglobin (Hb), and lactate dehydrogenase (LDH). As expected, this simplified model performed slightly better than the first minimal model by giving an AUC of 0.8.

From both equations (7) and (8), we can see that the non-linear effects are very significant. The non-linear coefficients for the second and third-order terms are in some cases higher than the linear terms and cannot be captured by a linear regression model. In many ways, our approach can be considered as a generalization of linear logistic regression. It is impressive that our minimal models of (7) and (8) are based on just 5 contributing factors.

D. Multimodality Model results

We provide comprehensive results from a large number of models in Table V. Here, we note that the models demanded significant computational resources. Even with 16 V100 32GB GPUs, it took us 1.5-2 months to train the different models on the large datasets described in section II. In Table V, we include results from logistic regression, the separable neural network (SNN), and XGB. We set the XGB model with a learning rate of 0.05, with 300 estimators, max depth of 4, and a subsample of 80%. We note that logistic regression is a special case of the SNN, where we use linear instead of cubic polynomials to describe the trends.

We show our use of low-parameter models in Table V. For example, the 3D CNN model for video analysis only

required 14,309 parameters. Similarly, the 1D CNN model for processing all the ECG traces only required 18,561 parameters. The combined model that uses all of EHR, Echo, and ECG only required 33,398 parameters. Our minimal models require just 25 or 20 parameters. Throughout our table, we can see a clear trade-off between lower accuracy achieved by minimal models (AUC: 0.76 and 0.78) and higher accuracy achieved by low-parameter unbiased multimodal models (max AUC: 0.88).

Unfortunately, we note that it is not possible to compare our low-parameter models to high-parameter models due to the fact that high-parameter models would require prohibitively larger training times.

We begin with the analysis of the results from individual modalities. We will then consider combinations of two or more modalities.

In terms of single modality models, echocardiography gave the best AUC at 0.86, closely followed by EHR at 0.85, and electrocardiography at 0.81. For echocardiography, video analysis significantly outperformed predictions that were solely based on measurements and findings. For EHR, the inclusion of all features significantly outperformed the use of age and sex alone. For ECG, the multichannel CNN model gave the best results that did not improve with the inclusion of ECG measurements and findings. Similar to echocardiography, the ECG CNN outperformed the ECG measurements and findings model, and the combination did not improve compared to the CNN. This suggests that the CNNs are finding important features in both echocardiography and ECG that we are not measured clinically.

The minimal models of equations (7) and (8) perform below the single modality models. Nevertheless, with AUCs of 0.78 and 0.80, they rival the performance of the electrocardiography model at 0.81. However, as mentioned earlier, the minimal models are far easier to understand and they can be implemented with simple at-home measurements or using 4 common blood panel measurements.

The multimodality models outperformed the single modality models. In the full model, the combination of all modalities gave the best performance with an AUC of 0.90. The full model was only slightly better than EHR+echocardiography (0.89) or EHR+electrocardiography (0.88). In terms of performance, XGB performed slightly better than SNN and logistic regression. However, in most cases, SNN performed almost at the same level as XGB. For the full model, SNN gave an AUC of 0.89 (compared to 0.90 for XGB).

The results from the single and multimodal models also outperformed our prior results on smaller datasets. In [12], the combination of echocardiography measurements and findings, and EHR studies using a random forest and 331,317 echocardiography gave an AUC of 0.85. In the current paper, the corresponding model would be EHR all + Echo m. that gave better AUC values at 0.86 with SNN, and 0.87 with XGB.

The multimodal model significantly outperformed a much smaller study described in [14]. In [14], the combination of echocardiography measurements and findings, video analysis from 24 views, and EHR data with 42,095 studies gave an AUC of 0.84. In the current paper, the corresponding model would be EHR all + Echo all that gave 0.88 with SNN and 0.89

TABLE V
MODEL PERFORMANCES IN PERCENT AUC MEASURED AT A RANDOMLY SELECTED ECHOCARDIOGRAPHY STUDY PER PATIENT. LR STANDS FOR LOGISTIC REGRESSION; SNN FOR SEPARABLE NEURAL NETWORK, THE PROPOSED METHOD; AND XGB FOR EXTREME GRADIENT BOOSTING.

	SNN Params	LR AUC	SNN AUC	XGB AUC
Echocardiography				
Echo measurements and findings	296	0.73	0.76	0.78
Videos using 3D CNNs	85854	0.84	0.84	0.86
Echo all	86150	0.85	0.85	0.86
Electrocardiography				
ECG measurements and findings	79	0.73	0.75	0.76
ECG traces using 1D CNN	18561	0.81	0.81	0.81
ECG all	18640	0.81	0.81	0.81
EHR				
Age + Sex	10	0.72	0.72	0.72
Age + Sex + EHR (EHR all)	153	0.82	0.84	0.85
EHR + Echocardiography				
Echo m. + Age + Sex	306	0.78	0.80	0.81
Videos + Age + Sex	85864	0.85	0.85	0.86
Echo all + Age + Sex	86160	0.85	0.86	0.87
EHR all + Echo m.	449	0.84	0.86	0.87
EHR all + Videos	86007	0.87	0.88	0.89
EHR all + Echo all	86303	0.87	0.88	0.89
EHR + Electrocardiography				
Age + Sex + ECG m.	89	0.79	0.81	0.81
Age + Sex + ECG tr.	18571	0.83	0.83	0.83
Age + Sex + ECG all.	18650	0.83	0.84	0.84
EHR all + ECG m.	232	0.84	0.86	0.87
EHR all + ECG tr.	18714	0.86	0.87	0.88
EHR all + ECG all	18793	0.86	0.87	0.88
EHR + Echocardiography + Electrocardiography				
Age + Sex + videos + ECG tr.	104425	0.87	0.87	0.88
EHR all + videos + ECG tr.	104568	0.88	0.89	0.90
EHR all + Echo m. + ECG m.	528	0.85	0.87	0.87
EHR all + Echo all + ECG m.	86382	0.88	0.89	0.89
EHR all + Echo all + ECG tr.	104864	0.88	0.89	0.90
EHR all + Echo all + ECG all*	104943	0.88	0.89	0.90
Minimal Models				
Age, Heart Rate, BMI, and Blood Pr	25	0.76	0.78	0.78
Age, LDH, Bilirubin, Lymphocytes and Hb	20	0.78	0.80	0.80

* Full model

with XGB. Here we note that we include six of the 24 views because of significant demands on compute time constraints. A model that includes all 24 views has the potential to further improve the overall performance.

In summary, the current paper introduces the use of separable neural networks to process a significantly larger dataset than was previously considered. The results for both single-modality and multimodality models have been significantly improved. In addition, the proposed separable neural network can be used to provide meaningful interpretations for different factors and across modalities. We note that the relationship between the dominant clinical factors and the overall risk is highly non-linear (see Fig. 2). In addition, we note that these non-linear relationships cannot be effectively captured by linear regression models.

V. CONCLUSION

The paper describes the development of separable models for risk assessment based on a massive multimodal dataset. The paper also develops the methodology that allows us to quantify the contribution of each clinical factor to the overall risk. For predicting all-cause 1-year mortality, the developed methods produced significantly better performance over prior models that used ECG, echocardiography, and EHR. The implementation code is provided in the DISIML package [24].

Our models have been validated on the largest dataset of its kind. For development and validation, the paper derives models based on 25,137,015 videos associated with 699,822 echocardiography studies from 316,125 patients, and 2,922,990 8-lead ECG traces from 631,353 patients. We also study the effectiveness of 84 low-parameter models. For all models, we support separable risk assessment that allows us to associate risk based on individual features. Furthermore, our separable models enable us to perform optimal feature selection based on the weights associated with each feature in the global model. The paper introduces a minimal model based on Age, Heart Rate, BMI, and Blood Pressure that can be monitored at home. At just 25 parameters, this minimal model achieves an AUC of 0.76. Based on optimal feature selection, we introduce an optimized minimal model based on Age, LDH, Bilirubin, Lymphocytes, and Hb. At just 20 parameters, our optimized minimal model achieves an AUC of 0.78. At an AUC of 0.78, the optimized minimal model performs better than the use of echo measurements and findings (AUC=0.76 with 296 parameters) and ECG measurements and findings (AUC=0.75 with 79 parameters). Nevertheless, our low-parameter 3D CNN performed significantly better (AUC=0.84 with 86k parameters). Overall, we have found that using additional information will improve performance. For the full multimodal model, with nearly 105k parameters, we have achieved an AUC of 0.89, a substantial improvement over our optimized minimal model.

REFERENCES

- [1] R. W. Foley, R. M. Maweni, L. Gorman, K. Murphy, D. J. Lundon, G. Durkan, R. Power, F. O'Brien, K. J. O'Malley, D. J. Galvin *et al.*, "European randomised study of screening for prostate cancer (erspc) risk calculators significantly outperform the prostate cancer prevention trial (pcpt) 2.0 in the prediction of prostate cancer: a multi-institutional study," *BJU international*, vol. 118, no. 5, pp. 706–713, 2016.
- [2] L. A. Allen, D. D. Matlock, S. M. Shetterly, S. Xu, W. C. Levy, L. B. Portalupi, C. K. McIlvennan, J. H. Gurwitz, E. S. Johnson, D. H. Smith *et al.*, "Use of risk models to predict death in the next year among individual ambulatory patients with heart failure," *JAMA Cardiology*, vol. 2, no. 4, pp. 435–441, 2017.
- [3] A. S. Panayides, M. S. Pattichis, S. Leandrou, C. Pitrakis, A. Constantinidou, and C. Pattichis, "Radiogenomics for precision medicine with a big data analytics perspective," *IEEE journal of biomedical and health informatics*, vol. early access, 2018.
- [4] C. Bonner, M. A. Fajardo, S. Hui, R. Stubbs, and L. Trevena, "Clinical validity, understandability, and actionability of online cardiovascular disease risk calculators: Systematic review," *Journal of Medical Internet Research*, vol. 20, no. 2, 2018.
- [5] M. W. Kattan, K. R. Hess, M. B. Amin, Y. Lu, K. G. Moons, J. E. Gershengwald, P. A. Gimotty, J. H. Guinney, S. Halabi, A. J. Lazar *et al.*, "American joint committee on cancer acceptance criteria for inclusion of risk models for individualized prognosis in the practice of precision medicine," *CA Cancer journal for clinicians*, vol. 66, no. 5, pp. 370–374, 2016.
- [6] P. W. Wilson, R. B. D'Agostino, D. Levy, A. M. Belanger, H. Silberzatz, and W. B. Kannel, "Prediction of coronary heart disease using risk factor categories," *Circulation*, vol. 97, no. 18, pp. 1837–1847, 1998.
- [7] S. Yadowsky, R. A. Hayward, J. B. Sussman, R. L. McClelland, Y.-I. Min, and S. Basu, "Clinical implications of revised pooled cohort equations for estimating atherosclerotic cardiovascular disease risk," *Annals of Internal Medicine*, vol. 169, no. 1, pp. 20–29, 2018.
- [8] W. C. Levy, D. Mozaffarian, D. T. Linker, S. Sutradhar, S. Anker, A. Cropp, I. Anand, A. Maggioni, P. Burton, M. Sullivan *et al.*, "The seattle heart failure model," *Circulation*, vol. 113, no. 11, pp. 1424–1433, 2006.
- [9] D. Ouyang, B. He, A. Ghorbani, N. Yuan, J. Ebinger, C. P. Langlotz, P. A. Heidenreich, R. A. Harrington, D. H. Liang, E. A. Ashley *et al.*, "Video-based ai for beat-to-beat assessment of cardiac function," *Nature*, vol. 580, no. 7802, pp. 252–256, 2020.
- [10] G. Duffy, P. P. Cheng, N. Yuan, B. He, A. C. Kwan, M. J. Shun-Shin, K. M. Alexander, J. Ebinger, M. P. Lungren, F. Rader *et al.*, "High-throughput precision phenotyping of left ventricular hypertrophy with cardiovascular deep learning," *JAMA cardiology*, vol. 7, no. 4, pp. 386–395, 2022.
- [11] C. D. Reddy, L. Lopez, D. Ouyang, J. Y. Zou, and B. He, "Video-based deep learning for automated assessment of left ventricular ejection fraction in pediatric patients," *Journal of the American Society of Echocardiography*, vol. 36, no. 5, pp. 482–489, 2023.
- [12] M. D. Samad, A. Ulloa Cerna, G. J. Wehner, L. Jing, D. Hartzel, C. W. Good, B. A. Williams, C. M. Haggerty, and B. K. Fornwalt, "Predicting survival from large echocardiography and electronic health record datasets: Optimization with machine learning," *JACC: Cardiovascular Imaging*, 2018.
- [13] S. Raghunath, A. E. Ulloa Cerna, L. Jing, D. P. VanMaanen, J. Stough, D. N. Hartzel, J. B. Leader, H. L. Kirchner, M. C. Stumpe, A. Hafez *et al.*, "Prediction of mortality from 12-lead electrocardiogram voltage data using a deep neural network," *Nature Medicine*, vol. 26, no. 6, pp. 886–891, 2020.
- [14] A. E. Ulloa Cerna, L. Jing, C. W. Good, D. P. vanMaanen, S. Raghunath, J. D. Suever, C. D. Nevius, G. J. Wehner, D. N. Hartzel, J. B. Leader *et al.*, "Deep-learning-assisted analysis of echocardiographic videos improves predictions of all-cause mortality," *Nature Biomedical Engineering*, vol. 5, no. 6, pp. 546–554, 2021.
- [15] S. v. Buuren and K. Groothuis-Oudshoorn, "mice: Multivariate imputation by chained equations in r," *Journal of Statistical Software*, pp. 1–68, 2010.
- [16] A. Farhangfar, L. Kurgan, and J. Dy, "Impact of imputation of missing values on classification error for discrete data," *Pattern Recognition*, vol. 41, no. 12, pp. 3692–3705, 2008.
- [17] D. P. Kingma and J. L. Ba, "Adam: A method for stochastic gradient descent," in *ICLR: international conference on learning representations*. ICLR US., 2015, pp. 1–15.
- [18] L. Prechelt, "Early stopping-but when?" in *Neural Networks: Tricks of the trade*. Springer, 1998, pp. 55–69.
- [19] A. E. Ulloa Cerna, L. Jing, J. M. Pfeifer, S. Raghunath, J. A. Ruhl, D. B. Rocha, J. B. Leader, N. Zimmerman, G. Lee, S. R. Steinhilb *et al.*, "recommend: an ecg-based machine-learning approach for identifying patients at high-risk of undiagnosed structural heart disease detectable by echocardiography," *Circulation*, 2021.
- [20] J. Friedman, T. Hastie, and R. Tibshirani, *The elements of statistical learning: Data Mining, Inference, and Prediction*, 2nd ed. New York: Springer series in statistics, 2009.
- [21] K. E. Rudd, S. C. Johnson, K. M. Agesa, K. A. Shackelford, D. Tsoi, D. R. Kievlan, D. V. Colombara, K. S. Ikuta, N. Kissoon, S. Finfer *et al.*, "Global, regional, and national sepsis incidence and mortality, 1990–2017: analysis for the global burden of disease study," *The Lancet*, vol. 395, no. 10219, pp. 200–211, 2020.
- [22] G. J. Wehner, L. Jing, C. M. Haggerty, J. D. Suever, J. B. Leader, D. N. Hartzel, H. L. Kirchner, J. N. Manus, N. James, Z. Ayar *et al.*, "Routinely reported ejection fraction and mortality in clinical practice: where does the nadir of risk lie?" *European heart journal*, vol. 41, no. 12, pp. 1249–1257, 2020.
- [23] J. E. Winter, R. J. MacInnis, N. Wattanapenpaiboon, and C. A. Nowson, "Bmi and all-cause mortality in older adults: a meta-analysis," *The American Journal of Clinical Nutrition*, vol. 99, no. 4, pp. 875–890, 2014.
- [24] A. Ulloa Cerna, "DISIML: deep learning library for tabular, series, and video data." <https://gitlab.com/alvarouc/disiml>, 2022.